



Article

Sol–Gel Synthesis and Characterization of YSZ Nanofillers for Dental Cements at Different Temperatures

Anastasia Beketova¹, Anna Theocharidou¹, Ioannis Tsamesidis¹, Athanasios E. Rigos¹, Georgia K. Pouroutzidou², Emmanouil-George C. Tzanakakis³, Dimitra Kourtidou², Liliana Liverani⁴, Marcela Arango Ospina⁴, Antonios Anastasiou⁵, Ioannis G. Tzoutzas³ and Eleana Kontonasaki^{1,*}

- ¹ Department of Prosthodontics, School of Dentistry, Faculty of Health Sciences, Aristotle University of Thessaloniki, 54124 Thessaloniki, Greece; anastasiabeketova@yahoo.com (A.B.); antheo@dent.auth.gr (A.T.); johntsames@gmail.com (I.T.); thanrigos@gmail.com (A.E.R.)
- ² School of Physics, Aristotle University of Thessaloniki, 54124 Thessaloniki, Greece; gpourout@physics.auth.gr (G.K.P.); dikourti@physics.auth.gr (D.K.)
- ³ School of Dentistry, National and Kapodistrian University, 10679 Athens, Greece; tzanakak@dent.uoa.gr (E.-G.C.T.); ioannistzoutzas@gmail.com (I.G.T.)
- ⁴ Department of Materials Science and Engineering, Institute of Biomaterials, University of Erlangen-Nuremberg, 91058 Erlangen, Germany; liliana.liverani@fau.de (L.L.); marcela.arango@fau.de (M.A.O.)
- ⁵ Department of Chemical Engineering and Analytical Science, University of Manchester, Manchester M13AL, UK; antonios.anastasiou@manchester.ac.uk
- * Correspondence: kont@dent.auth.gr; Tel.: +30-2310-999517



Citation: Beketova, A.; Theocharidou, A.; Tsamesidis, I.; Rigos, A.E.; Pouroutzidou, G.K.; Tzanakakis, E.-G.C.; Kourtidou, D.; Liverani, L.; Ospina, M.A.; Anastasiou, A.; et al. Sol–Gel Synthesis and Characterization of YSZ Nanofillers for Dental Cements at Different Temperatures. *Dent. J.* **2021**, *9*, 128. <https://doi.org/10.3390/dj9110128>

Academic Editor: Andrea Scribante

Received: 17 September 2021
Accepted: 26 October 2021
Published: 29 October 2021

Publisher's Note: MDPI stays neutral with regard to jurisdictional claims in published maps and institutional affiliations.



Copyright: © 2021 by the authors. Licensee MDPI, Basel, Switzerland. This article is an open access article distributed under the terms and conditions of the Creative Commons Attribution (CC BY) license (<https://creativecommons.org/licenses/by/4.0/>).

Abstract: Background: Yttria-stabilized zirconia nanoparticles can be applied as fillers to improve the mechanical and antibacterial properties of luting cement. The aim of this study was to synthesize yttria-stabilized zirconia nanoparticles by the sol–gel method and to investigate their composition, structure, morphology and biological properties. Methods: Nanopowders of ZrO₂ 7 wt% Y₂O₃ (nY-ZrO) were synthesized by the sol–gel method and were sintered at three different temperatures: 800, 1000 and 1200 °C, and their composition, size and morphology were investigated. The biocompatibility was investigated with human gingival fibroblasts (hGFs), while reactive oxygen species (ROS) production was evaluated through fluorescence analysis. Results: All synthesized materials were composed of tetragonal zirconia, while nanopowders sintered at 800 °C and 1000 °C additionally contained 5 and 20 wt% of the cubic phase. By increasing the calcination temperature, the crystalline size of the nanoparticles increased from 12.1 nm for nY-ZrO800 to 47.2 nm for nY-ZrO1200. Nano-sized particles with good dispersion and low agglomeration were received. Cell culture studies with human gingival fibroblasts verified the nanopowders' biocompatibility and their ROS scavenging activity. Conclusions: the obtained sol–gel derived nanopowders showed suitable properties to be potentially used as nanofillers for dental luting cement.

Keywords: nanoparticle; chemical precipitation; yttrium; zirconium; gingival fibroblasts; toxicity tests; oxidative stress

1. Introduction

Various nanoparticles have been proposed for the reinforcement of different dental materials such as restorative composite materials, glass ionomer cement, dental adhesives and calcium silicate cement. Among them, silica, alumina, glass and metal oxide nanoparticles led to improved commercial products with enhanced mechanical properties. In the last two decades, high purity zirconia (ZrO₂) nanomaterials gained significant interest in dental technology, as they combine high toughness, high strength and high corrosion resistance with biocompatibility, lack of toxicity and antibacterial properties [1]. Although their primary application is in the fabrication of dense polycrystalline zirconia ceramics in the form

of dental crowns, fixed partial dentures, implants, implant abutments, posts, orthodontic brackets, etc. [2,3], they have also been proposed as nano-filling materials [4,5] and nanocoatings [6,7], while due to their opaque white nature, they can also serve as radiopacity elements in cement [8] and root filling materials [9]. Zirconia filler nanoclusters with particle sizes ranging from 20 to 75 nm were used for strengthening commercial restorative dental composites such as Filtek Z250 and Harvard ZirkonCore [4]. The incorporation of ZrO₂ nanoparticles in various matrices can result in composite materials with significantly improved flexural strength, fracture toughness and shear bond strength [10,11]. Due to their antibacterial properties, they could also be applied as fillers in various dental care materials such as toothpaste, lining materials and dental cement [12,13]. The reinforcement of resin luting cement by ZrO₂-based nanofillers could be beneficial for the establishment of durable bonds with zirconia fixed restorations.

Zirconium oxide presents with three temperature-dependent crystal phases: monoclinic (m-ZrO₂) is thermodynamically stable at room temperature and up to 1100 °C, tetragonal (t-ZrO₂) between 1100 and 2370 °C and cubic (c-ZrO₂), which is found at a higher temperature above 2370 °C [14,15]. Tetragonal zirconia presents with the most favorable mechanical properties due to the phenomenon of toughening transformation, i.e., its transformation under moisture and stress to the thermodynamically stable at room temperature monoclinic phase [16]. During the cooling of the material at 950 °C, conversion from the tetragonal to the monoclinic (t→m) form takes place [17]. This phase transformation is accompanied by a volume increase of ~4% [18]. A different transformation (c→t) can cause the creation of a different tetragonal phase (t'), which is rich in yttrium with a smaller crystal size and higher resistance to the t→m phase transformation [19]. In order to stabilize tetragonal zirconia at room temperature, various doping elements were tested, such as cerium, yttrium, calcium, magnesium, etc., and yttrium is the most utilized. Yttrium stabilized tetragonal zirconia (YSZ) has attracted worldwide interest as it presents high strength and toughness [20].

Various methods were proposed for the synthesis of zirconia nanopowder [21]. The most effective ones are wet-chemical synthesis approaches, such as sol-gel, co-precipitation and hydrothermal routes [22–25]. Using sol-gel synthesis, uniform, nano-sized powders with high purity can be produced [26]. This process is based on the hydrolysis and subsequent condensation reactions of inorganic salts and metal-organic compounds. These reactions lead to the formation of a sol which is converted into a gel. The gel is further processed with calcination at various temperatures to obtain a homogenous nanopowder. In the co-precipitation method, an aqueous solution is prepared where zirconia precursors are diluted, and then a chemical precipitant agent is added for the effective precipitation of metal hydroxides. The precipitated powder is subsequently rinsed, filtered and dried before calcination at various temperatures to receive the desired crystalline phases. The nucleation and growth mechanisms can be monitored by modifying the solution's pH and temperature. It is an effective and low-cost method, although it generally results in a wide particle size distribution and agglomeration [27]. Hydrothermal routes usually involve water as the solvent and an initial co-precipitation at high temperatures and pressure in sealed containers to obtain a crystalline powder. It is also a low-cost and ecological method resulting in homogenous products, although presenting similar drawbacks of co-precipitation such as high agglomeration, which results in poor sinterability [28,29]. All of these methods necessitate precise control of all the involved parameters (pH, time, temperature, etc.) to receive the desired size and crystalline nature of nanoparticles. Nanoparticles with an average size below 50 nm were suggested as appropriate zirconia nanofillers in dental restorative composites and cement [13,30].

Despite the fact that pure monoclinic zirconia nanoparticles have been used as fillers in many dental materials [7], YSZ nanoparticles with tetragonal structure at room temperature have only scarcely been evaluated [31,32], although they may show higher enhancement of the mechanical properties of dental composites and cement. The aim of this study was to synthesize yttria-stabilized zirconia (YSZ) nanopowders, to be used as nanofillers

in dental cement by the sol–gel method and to investigate the impact of different sintering temperatures on their crystal structure, morphology and biocompatibility. The null hypothesis was that sintering temperature would not affect the biocompatibility of the synthesized materials.

2. Materials and Methods

2.1. Synthesis of Nanoparticles

ZrO₂ 7 wt% Y₂O₃ nanoparticles were synthesized by the sol–gel method using zirconium oxychloride octahydrate (ZrOCl₂ 8H₂O) and yttrium nitrate hexahydrate (Y(NO₃)₃ 6H₂O) as starting materials [33,34]. Raw materials were dissolved in double distilled water, mixed and then an aqueous solution of ethylene glycol and an aqueous citric acid concentrate was added under heating and stirring. The molar ratios of citric acid:metal and citric acid:ethylene glycol were 3.65 and 1, respectively. The materials were heated stepwise to the temperatures of 100 °C, 200 °C and 300 °C for 3 h/each to eliminate organic materials [33]. The obtained gel was sintered at three different temperatures: 800, 1000 and 1200 °C for 2 hours after differential thermal and thermogravimetric analyses (DTA/TG). The obtained calcinated materials were ground in a mortar into fine powders (nY-ZrO800, nY-ZrO1000, nY-ZrO1200).

2.2. Differential Thermal and Thermogravimetric Analysis (TG-DSC)

The thermal behavior of the dried gel was investigated by Thermogravimetric Analysis and Differential Scanning Calorimetry (TG-DSC) performed in dry air from room temperature up to 1300 °C, with a heating rate of 10 °C min⁻¹ (SETSYS 16/18, SETARAM, Lyon, France). The sample (≈35 mg) was placed in alumina crucibles while an empty alumina crucible was used as a reference.

2.3. Fourier Transform Infrared Analysis (FTIR)

The FTIR transmittance spectra of the nanoparticles sintering were obtained by the KBr technique. A Spectrometer (Spectrum 1000, PerkinElmer, Inc., Waltham, MA, USA) was employed measuring in the MIR region (4000–400 cm⁻¹) with a resolution of 4 cm⁻¹ and performing 32 scans per spectrum.

2.4. X-Ray Diffraction Analysis (XRD)

The XRD analysis of the nanoparticles was performed using a diffractometer (Rigaku Ultima, Rigaku, Japan) with Ni-filtered CuKα radiation ($\lambda = 0.1542 \text{ \AA}$). A 2θ range of 5–90° was measured, with a scanning speed of 0.05 ° 2 θ /s, 1.5 s per step. The ICDD PDF-4+ (2009) database was used for the identification of the phases contained in the studied samples. The crystallite size was calculated with the Scherer's formula: $D = 0.89\lambda / \beta \cos\theta$, where D is the crystallite size (nm), λ is the wavelength of X-ray beam (nm), β is the full width at the half maximum of the main peak, and θ is the diffraction angle (°). Rietveld analysis of XRD patterns was performed to quantify the crystalline phase contents.

2.5. Scanning Electron Microscopy-Energy-Dispersive X-ray Spectroscopy (SEM/EDX)

The morphology of all samples was determined by Scanning Electron Microscopy SEM (Auriga Base, Carl-Zeiss) associated with an energy dispersive X-ray (EDX) analyzer (X-Max^N, Oxford Instruments, Abingdon, UK) to detect their chemical composition during SEM observation.

2.6. Transmission Electron Microscopy (TEM)

For TEM imaging, the NPs samples were dispersed in ethanol and placed in an ultrasonic bath for 10 min. Then, a drop of the suspension was placed onto a Lacey Carbon Film (Agar Scientific Ltd., Stansted, UK). For imaging and morphology analysis of nanoparticles, a latest-generation Field Emission Gun Transmission Electron Microscope (Talos F200X) was utilized. The mean particle size of the samples was determined by

measuring the size of 50 particles. The exact distance from the central spot and each one of the diffracted spots was measured in program Image J. Experimental interplanar spacing (d) was estimated from the formula: $d_{\text{spacing}} = \lambda L/R$ [35,36].

2.7. Dynamic Light Scattering Analysis (DLS)

Dynamic light scattering (Zetasizer Nano ZS) was used for the estimation of hydrodynamic size and polydispersity index (PDI) of the nanoparticles. Measurements were performed at 25 °C after 5 min sonication of the samples that contained the different nanoparticles dispersed in distilled water at a concentration of 1 g/L.

2.8. Establishment of Primary Cell Cultures

Human gingival fibroblasts were grown in primary culture from free gingiva biopsies received from young, healthy donors after extraction of their third molars. The Institutional Ethical Committee approved the protocol (#35/07-05-2018), and volunteer patients signed their informed consent forms before extractions. In brief, gingival tissue biopsies were placed in 25 cm² culture flasks with Dulbecco modified Eagle medium (DMEM, Invitrogen) supplemented with 10% Fetal Bovine Serum (FBS, Invitrogen) and penicillin (100 units/mL), streptomycin (100 mg/mL) and Amphotericin B (0.25 mg/mL) to allow the outgrowth of cells. The flasks were incubated at 37 °C in a humidified atmosphere with 5% CO₂, and the medium was replaced twice a week. When the primary cell culture reached confluence (70–80% of the flask), cells were detached with trypsin, transferred to a larger 75 cm² flask (passage 1) and then subcultured for further experiments. Cells from the 5th and 6th passages were used for all experiments.

2.9. Evaluation of Cell Viability by the MTT Assay

Mitochondrial activity evaluation of human gingival fibroblasts with nY-ZrO was performed using the MTT assay (3-(4,5-dimethylthiazol-2-yl)-2,5-diphenyltetrazolium bromide). Cells were seeded in 96 well-plates (3×10^4 cells/well) and left 24 h to attach in a 5% CO₂ incubator at 37 °C. A stock solution of 2 mg of NPs per 1 mL of culture medium was prepared, and a series of dilutions with nanoparticles at different concentrations (0.1, 0.25 and 0.5 mg/mL) were evaluated after 24 and 72 h of incubation. Those concentrations were selected based on previous studies on the toxicity of various nanoparticles [37–39]. Untreated cells served as a positive control, while cells cultured with a culture medium without fetal bovine serum served as a negative control. The proliferation of the cells was calculated by measuring the mitochondrial dehydrogenase activity of living cells, which was verified by the transformation of the yellow tetrazolium salt into blue formazan crystals by using dimethyl-sulfoxide (DMSO) (Sigma Aldrich, St. Louis, MO, USA) as dissolvent. Optical density was determined spectrophotometrically by a microplate reader (Epoch, Biotek, Biotek Instruments, Inc, Winooski, VT, USA). Measurements were performed at a wavelength of 545 nm with a reference filter at 630 nm. Experiments were performed in triplicates. The results were expressed as % percentage of the control average optical density value.

2.10. Fluorescence Analysis for the Detection of ROS Levels

The cell-permeable ROS-sensitive probe 2',7'-dichlorodihydrofluorescein diacetate (H2DCFDA) was used for the detection of reactive oxygen species [40], which fluoresces at 520 nm ($\lambda_{\text{ex}} 480$ nm) upon oxidation. A stock solution of 0.5 mM H2DCFDA in DMSO was prepared. In order to avoid autofluorescence, controls were prepared without H2DCFDA but only with its solvent, DMSO. The probe was added to the well plates of human gingival fibroblasts treated at different concentrations of yttria-stabilized zirconia nanofillers for 24 and 72 h and left to incubate for 30 min (oxidation). Measurement of the fluorescence was performed after transferring the desired suspensions in 96-well black microplates using a SAFAS Xenius fluorometer. The relative fluorescence is expressed as “% maximal emission” as determined with the software “Xenius”.

2.11. Statistical Analysis

Statistical analysis of the cell viability and ROS levels data was performed with the Paired Samples *t*-Test using the SPSS software. The level of statistical significance was set at 0.05 ($p < 0.05$).

3. Results

3.1. TG-DSC Analysis

The mass loss along with its first derivative (dTG) and the heat flow curves of the prepared gel is presented in Figure 1.

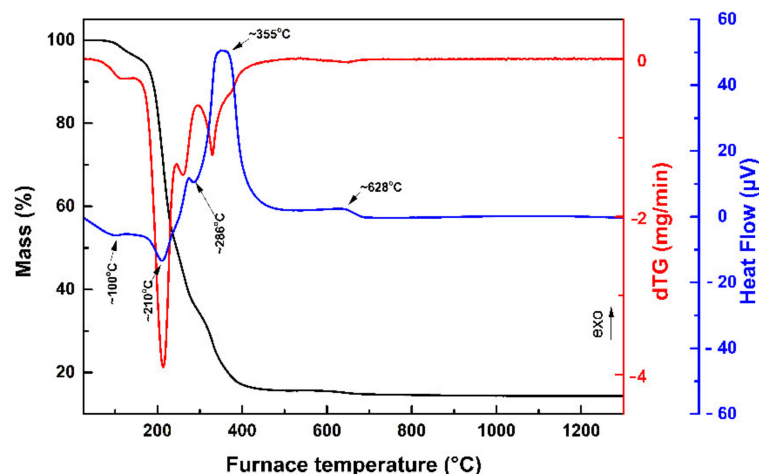


Figure 1. TG, dTG and Heat Flow curves of the gel at 10 °C/min heating rate in dry air.

From the dTG curve, it can be concluded that the overall weight loss (85.3%) occurred in five main stages. The first step took place at temperatures between 26 and 150 °C, accompanied by an endothermic peak at ~100 °C, and is attributed to the evaporation of the absorbed water (3.5% mass loss) [33,34,41,42]. In the temperature range of 150–240 °C, the second step of the degradation presented an endothermic peak at ~210 °C that can be ascribed to the release of nitrates and/or the citrate matrix's decomposition (45% mass loss) [43,44]. The third stage of the gel's degradation occurred around 240–300 °C with an endothermic peak appearing at ~286 °C, possibly due to the decomposition of zirconyl oxalate ($ZrOC_2O_4$) and $Y_2(C_2O_4)_3$ (20.9% mass loss) [43,45]. An exothermic peak at ~355 °C took place on the fourth step of the process, which took place at temperatures between 300 and 540 °C. This peak could be attributed to the degradation of organic and organometallic compounds, CO_2 removal and the destruction of the polymeric network [34] or to the oxidation of the residual organic compounds [44] (mass loss 15.9%). During the final step of the degradation that occurred in the temperature range of 540–900 °C, an exothermic peak appeared at ~628 °C, possibly related to the removal of the element carbon from the final compound [44] and/or a crystalline–amorphous phase transition [33,45].

3.2. FTIR Analysis

Infrared vibrational spectra of Y-Zr powders, sintered at temperatures 800, 1000 and 1200 °C, are presented in Figure 2. FTIR transmission spectra of all the specimens showed broad bands at about 430–440 cm^{-1} and a weak broad band at around 600–650 cm^{-1} characteristic for the tetragonal phase [46]. Apparently, no monoclinic phase was detected in none of the specimens because of the absence of the distinctive sharp band for this phase at 740 cm^{-1} . Low-intensity peaks at 1400 and 1650 cm^{-1} of nY-ZrO800 specimen might be attributed to the symmetric and asymmetric stretching vibrations of the carboxylate groups of organic components of decomposed gel [34].

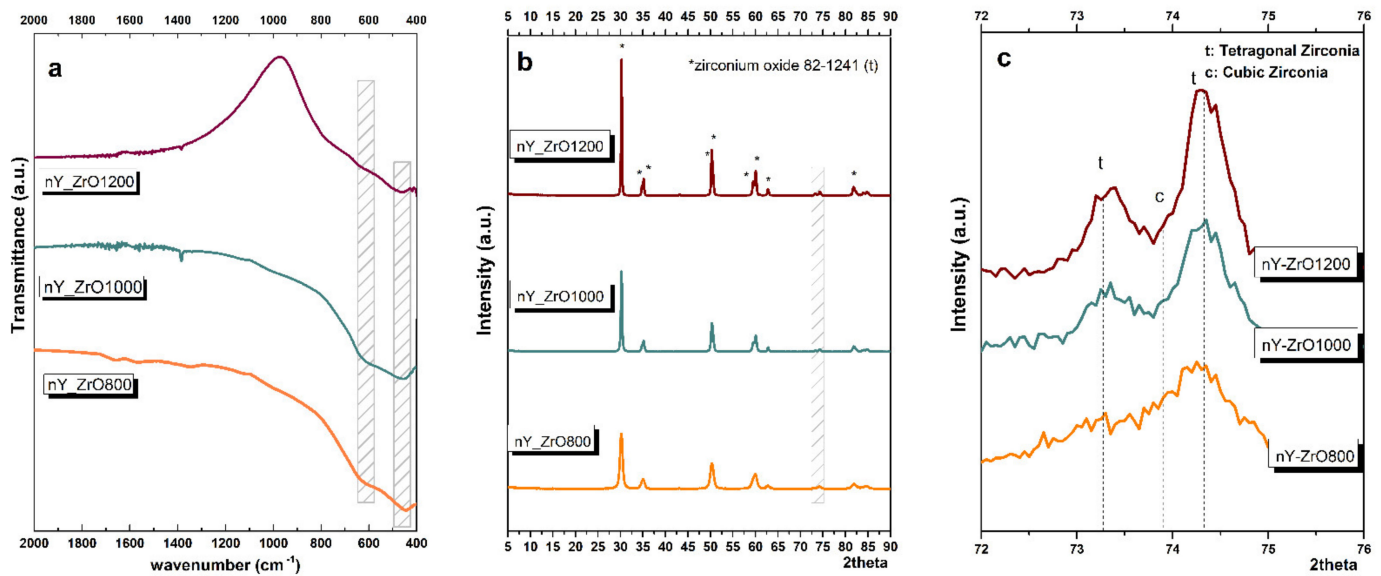


Figure 2. (a) FTIR; (b) XRD analysis of the zirconia nanoparticles sintered at 800, 1000 and 1200 °C, respectively. Higher magnification of XRD patterns in the area of 72–76 2θ is presented in (c) to unravel the splitting of the peaks due to the presence of the tetragonal phase.

3.3. XRD Analysis

The XRD patterns of the three experimental materials are displayed in Figure 2, while the percentages of crystalline phases are presented in Table 1. The diffraction peaks of all nY-ZrO1200 specimen show the formation of pure tetragonal zirconium yttrium oxide $Zr_{0.9}Y_{0.1}O_{1.95}$ without any detectable secondary phases. The distinguishing characteristic peaks for tetragonal zirconia phase occur at $2\theta = 30$ to 45 for the (111), (002), (200), (202) and (112); at $2\theta = 45$ to 65 for the (202), (220), (113), (311) and (222); and at $2\theta = 72$ to 85 for (004), (400), (331), (313), (420) and (402) reflections [47,48]. It is important to mention that the double peak around 73.2 and 74 2θ angles are characteristic for tetragonal zirconia crystal [48,49]. Specimens nY-ZrO1000 and nY-ZrO800 also contain ~5% and ~20% of cubic zirconium yttrium oxide, respectively. By increasing the sintering temperature from 800 to 1000 and 1200 °C, the peaks appeared sharper and more intense. At the same time, the full width at half maximum (FWHM) of diffraction pattern became narrower, indicating increased crystallinity of the specimens. Thus, the crystallite size of YSZ nanoparticles calculated by the Sherrer equation was 12.1nm for nY-ZrO800, 29.2nm for nY-ZrO1000 powder and 47.2nm for nY-ZrO1200.

Table 1. Content of tetragonal (t) and cubic (c) crystalline phases in wt% sintered specimens.

Specimen	t	c
nY-ZrO800	79.65%	20.35%
nY-ZrO1000	95.13%	4.87%
nY-ZrO1200	100.00%	0%

3.4. SEM/EDX

SEM analysis (Figure 3) in high magnifications ($100,000\times$) showed the fine submicron-sized (~10–15 nm) particles with uniform spherical morphology in nY-ZrO800 specimens. With the increase in sintering temperature to 1000 °C, grains become bigger in size (30–50 nm) and have a low agglomerated microstructure. Finally, specimens sintered at 1200 °C seem more agglomerated and have polyhedral morphology with particle sizes of more than 100 nm. EDX analysis of three specimens detected Zr, Y and minor traces of Hf, with a Y/Zr ratio around 0.06–0.07.

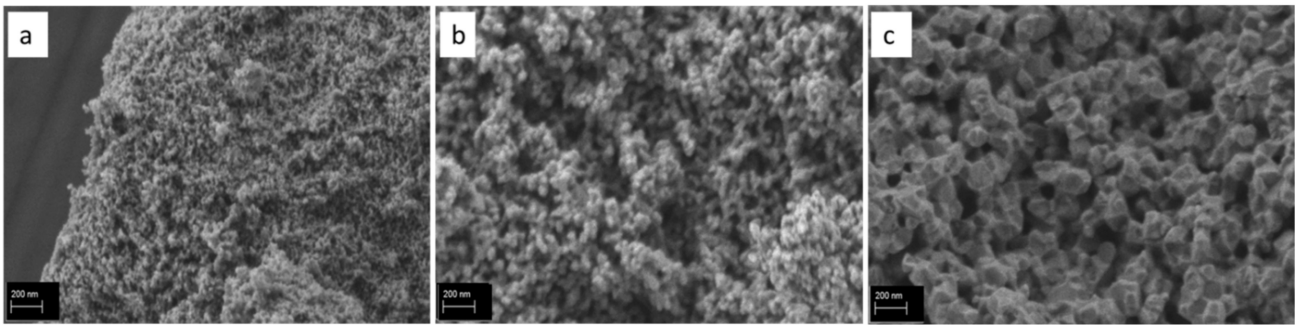


Figure 3. SEM images of the nY-ZrO powders sintered at 800 ((a)-nY-ZrO800), 1000 ((b)-nY-ZrO1000) and 1200 °C ((c)-nY-ZrO1200), showing increase in crystalline size with increase in sintering temperature.

3.5. TEM

The obtained TEM image of nY-ZrO powders sintered at 1000 °C is shown in Figure 4a. The observed nanoparticles are uniform, homogeneously distributed and well defined. Their morphology is polyhedral, and their size ranges between 9 and 53 nm, with an average calculated particle size of 28.4 nm (± 11 nm). In images with higher resolution (Figure 4b), crystal lattice could be observed, while dark inclusions indicate well-crystallized grains. The electron pattern of crystals corresponds to pure tetragonal zirconia, which can be estimated from calculations of interplanar spacings. (Table 2).

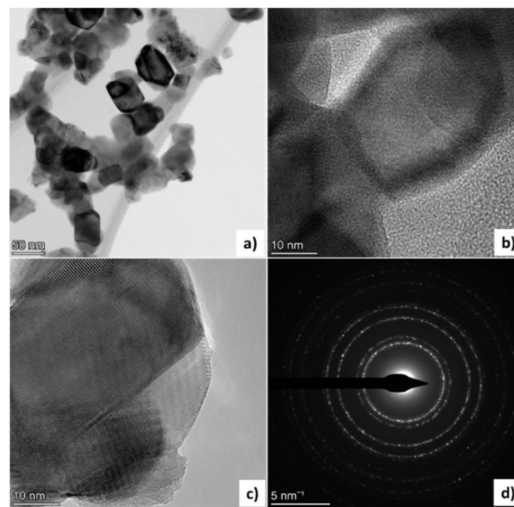


Figure 4. TEM image showing morphology of nanoparticles sintered at 1000 °C (a–c), and electron diffraction pattern (d).

Table 2. Experimental and theoretical d -value (interplanar spacing) of the phase identified as tetragonal Zirconia (Identification Card Number# 82-1241).

Ring	Diam. cm	R cm	$d_{\text{spac}} \text{ \AA}$	ICDD #82-1241	St.Dev.	St.Dev %	hkl
Ring 1	6.5	3.250	2.892	2.963	0.0239	2.3924	101
Ring 2	7.6	3.800	2.474	2.559	0.0332	3.3151	110
Ring 3	10.3	5.150	1.825	1.818	0.0043	0.4260	112
Ring 4	12.45	6.225	1.510	1.544	0.0221	2.2058	103
Ring 5	13	6.500	1.446	1.482	0.0239	2.3924	202
Ring 6	15.65	7.825	1.201	1.212	0.0085	0.8503	104
Ring 7	17.35	8.675	1.084	1.144	0.0530	5.2986	310

3.6. DLS

The average size of all synthesized powders, analyzed by Dynamic Light Scattering techniques (DLS), were estimated 243.9 nm for nY-ZrO800, 188.96 for nY-ZrO1000 and 364.00 for nY-ZrO1200 (Table 3). The low polydispersity index, especially in the nY-ZrO 800 and nY-ZrO1000 samples (<0.28), indicates narrow size distribution of grains and good quality of the obtained materials.

Table 3. Results from DLS analysis.

Specimen	Size (d.nm)	Standard Deviation	%Std Deviation	Pdl
nY-ZrO800	243.890	2.345	0.961	0.265
nY-ZrO1000	188.956	5.831	3.086	0.277
nY-ZrO1200	364.003	8.216	2.257	0.376

3.7. Evaluation of Cell Viability

MTT assay of the tested specimens (Figure 5) showed that nY-ZrO1000 and nY-ZrO1200 presented a biocompatible biological behavior as compared to the positive control in 24 and 72 h ($p < 0.001$). The lowest cell viability/proliferation was found in the highest concentrations of nanoparticles (0.5 mg/mL) in all the experimental groups ($p < 0.001$). The most pronounced and statistically significant increase in cell viability ($p < 0.001$) was reported for cells treated with 0.1 mg/mL of nY-ZrO1000 after 24 h of incubation. The lowest optical density values were recorded in the nY-ZrO800 group at 72 h, suggesting its mildly toxic behavior. Time dependence and dose dependence were not observed for the experimental dose and time points, except for cells treated with nY-ZrO1200 after 72 h of incubation, presenting a statistically significant dose-dependent behavior ($p < 0.05$).

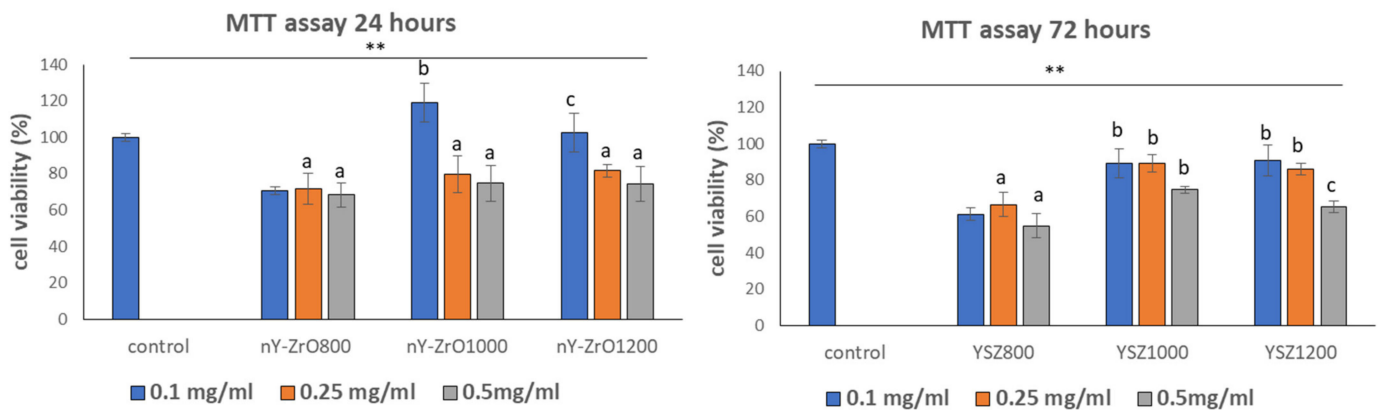


Figure 5. MTT results of cell viability at different concentrations (0.1, 0.25, 0.5 mg/mL) of yttria stabilized zirconia nanofillers. ** Indicates statistically significant difference ($p < 0.001$) between treated and untreated cells without nanoparticles (control), while different letters suggest statistically significant differences ($p < 0.001$) among concentrations.

3.8. Fluorescence Analysis for the Detection of Reactive Oxygen Species Levels

Figure 6 illustrates that after 24 h of incubation, all specimens showed a statistically significant reduction of reactive oxygen species as compared to the control ($p < 0.001$). After 72 h, in nY-ZrO1000 and nY-ZrO1200 specimens, a significant reduction in reactive oxygen species levels was observed, which was not dependent on NP concentrations ($p < 0.01$). Higher antioxidant activity of YSZ800 nanoparticles was observed at the 72h time point in the concentration of 0.25 mg/mL, indicating its antioxidant properties.

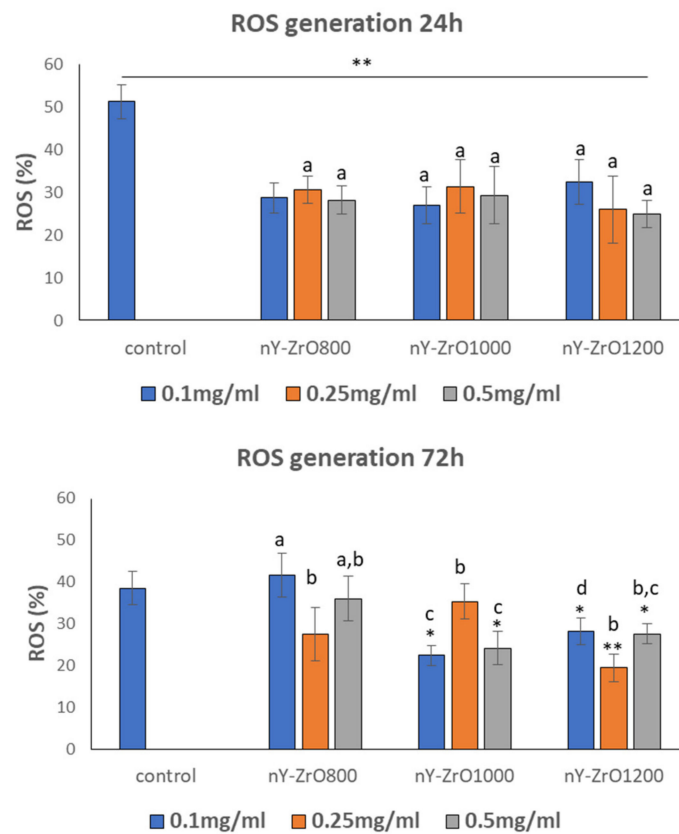


Figure 6. Reactive oxygen species (ROS) measured using H2DCFDA in HGF cells treated for 24 and 72 h at different concentrations (0.1, 0.25, 0.5 mg/mL) of yttria-stabilized zirconia nanofillers. * Indicates statistically significant difference ($p < 0.05$) between treated and untreated cells without nanoparticles (control), ** indicates statistically significant difference ($p < 0.0001$) between treated and untreated cells without nanoparticles, while different letters suggest statistically significant differences ($p < 0.001$) among concentrations.

4. Discussion

Because of the favorable properties of zirconia nanoparticles, their synthesis has attracted wide scientific interest over the years, and various methodologies were applied to optimize their size, crystalline state and morphology, depending on the targeted application [7]. ZrO₂ and particularly YSZ nanoparticles present high ionic conductivity, mechanical strength, chemical inertness, high melting point, low thermal conductivity [50] as well as biocompatibility [51], characteristics that make zirconia nanoparticles attractive for a wide range of applications. Yttria-stabilized zirconia nanoparticles offer multiple advantages compared to pure ZrO₂ in terms of high mechanical properties, antibacterial properties and low thermal conductivity that make them attractive candidates for fillers in dental cement and composite materials [52,53].

In the present study, YSZ nanoparticles were synthesized with the sol-gel technique based on the Pechini method, as described previously by Hajizadeh-Oghaz [24]. In their study, spherical tetragonal nanoparticles were synthesized with an average size of 29 nm, as determined by Scherrer's formula. This size corresponds to calcination at 1000 °C and is in close agreement with the results of the present study (28.4 nm). Calcination temperature was found to be the most important factor influencing particle size of YSZ, as also pointed out in similar studies [24,33,54]. For example, Maridurai et al. [54] synthesized YSZ nanoparticles by the co-precipitation method and observed an average particle size of 17 nm with TEM analysis and predominantly spherical shape after calcination at 700 °C. Although a different technique was used for the synthesis, Scherrer's equation indicated an average size of 12 nm [54], similar to the size of nanoparticles in the present study after

calcination at 800 °C. However, in the study of Maridurai et al. [54], cubic zirconia was the predominant crystalline phase and not the tetragonal one, as in the present study.

Apart from yttrium, other elements were used to stabilize tetragonal ZrO₂ nanoparticles, such as ytterbium (Yb) and gadolinium (Gd) [55]. With these elements, XRD revealed an increase in size with temperature, as an average size of 19 nm was calculated when calcination was performed at 600 °C and 43 nm following calcination at 1000 °C [55]. This finding was also observed in the present study and is justified by the temperature-induced grain growth and densification. As shown by SEM micrographs in Figure 3, heating at 1200 °C led to significant consolidation of the particles.

Khajavi et al. [56] recently synthesized and evaluated Ce-Y co-doped zirconia nanoparticles by the hydrothermal method, which presented a spherical shape and average size of 8.6 nm after calcination at 900 °C. In addition, the authors reported that a predominantly tetragonal phase of zirconia was detected [56], which is in agreement with the present study, although their nanoparticles presented a smaller average size. They also emphasized the significance of retaining the tetragonal phase after heat treatment, which is correlated to mechanical properties enhancement through the transformation toughening mechanism. In the present study, the tetragonal phase is well retained at all temperatures, as verified by the double peaks of the (002)/(200), (113)/(311), (400)/(004) and (402)/(420) planes in the XRD pattern of the nY-ZrO1000 and TEM analysis of the nY-ZrO1000 [48,49]. The broadening of the respective peaks in the pattern of the nY-ZrO800 suggests peak overlapping [48], which is a common finding, as in X-ray diffraction analysis, the cubic and tetragonal structures cannot be easily distinguished [48]. A high amount of tetragonal zirconia and no monoclinic phase were found at 800 °C, quite below the phase equilibrium (1175 °C), which can be justified by the nano-scale size of powders that present high surface area. After the studies of Garvie [57], which suggested that 30 nm of crystalline size is the critical factor for the stabilization of the tetragonal phase at lower temperatures, many studies suggested that an even smaller size (18 nm [58] or 10 nm [59]) of zirconia nanocrystals do not inhibit its stabilization, depending on various parameters such as interfacial energy, strain energy, hydrostatic pressure, water vapor, ion doping, oxygen vacancies, etc. [60]. Therefore, these critical size factors are strictly applicable only for strain-free ZrO₂ nanocrystallites of spherical or near-spherical shape in contact with air at ambient pressure and temperature. In the present study, the average size calculated by XRD was below 30 nm at temperatures below 1000 °C, which corroborates well with the proposed theories [60]. Similarly, Tailor et al. [34] synthesized YSZ nano-clusters for thermal insulation by the sol-gel method and, in agreement with our study, mainly detected the tetragonal phase of YSZ and average particle size of around 40 nm. In the present study, a very small amount of cubic phase was calculated by the Rietveld method (<5%) for the nYZ-1000, which was reported in cases of ultrafine crystallites, in the range of 2–20 nm [61,62] and in doped YSZ nanoparticles [56].

Nanoparticles are prone to spontaneous agglomeration due to high specific surface area. This surface area is responsible for the lowering of the sintering temperature of nanoparticles compared to the sintering temperature of their micro-sized counterparts [63]. It was shown that the activation energy for densification of ZrO₂ nanoceramics is 50% less than that of submicron ZrO₂ [64]. Stolzenburg et al. [65], using a solvothermal synthesis method, observed ZrO₂ nanoparticles agglomerates of size around 200 nm and justified their results by a probable instantaneous self-arrangement of nanoparticles after nucleating in the tetragonal phase. In the present study, the respective values were 243.9 nm, 188.96 nm and 364.00 nm, following heating at 800, 1000 and 1200 °C, respectively. At high temperatures, particles draw near and neck-shape junctions between adjacent nanoparticles permit densification and pore shrinkage, as in the case of nY-ZrO1200. DLS measurements in the present study suggest a moderate to low polydispersity in all samples, as the polydispersity index (PDI) values are below or around 0.3, but the high average nanoparticle diameter calculated may be attributed to the tendency of nanoparticles to assemble in nanoclusters or to the severe distortion of DLS measurements due to nanoparticles poly-

hedral morphology [66,67]. Considerably larger nanoparticles sizes compared to TEM and SAXS were recorded by DLS [68], and even slight soft agglomeration or a small percentage of larger particles can significantly increase the DLS calculated particle size distribution [66,67].

In order to investigate the biocompatibility and antioxidant activity of the experimentally obtained yttria-zirconia nanoparticles, MTT assay and fluorescence analysis for detection of ROS levels were performed. Nanoparticles sintered at higher temperatures of 1000 and 1200 °C showed biocompatible behavior and thus are not expected to cause any adverse effects after their addition to luting cement. Nanoparticles sintered at 800 °C presented mildly toxic behavior, probably due to finer particle size as evidenced from the SEM microphotograph (Figure 3a). Nanoparticles of small size <10 nm can either penetrate the cell membrane or enter the nucleus, thus being mildly or heavily toxic [69]. Pan et al. [70] reported that gold NPs of 15 nm in size were 60 times less toxic than 1.4 nm NPs for fibroblasts, epithelial cells, macrophages and melanoma cells. In agreement with our study, Zhang et al. [71] reported in vitro cytocompatibility of ZrO₂ nanopowders (<50 nm) with MG-63 cells and L929 fibroblasts in a dose-dependent manner. Cell culture studies with human umbilical vein endothelial cells (HUVECs) cultured with 500 µg/mL (4.06 mM) of ZrO₂ nanoparticles (30–40 nm) also showed relatively high cell viability (>80%) [72]. In a study by Rutherford et al. [73], YSZ nanoparticles (approximately 7 nm) with different molar concentrations of yttria and nano-sized ZrO₂ showed biocompatible behavior with bone marrow mesenchymal stem cells. Even at a high concentration of nanoparticles, cells maintained their morphology. Further research is needed to elucidate the underlying factors and mechanisms affecting zirconia nanoparticles' cytotoxicity at different cell lines. In general, immediately after nanoparticles' contact with the biological environment, a certain layer of proteins will adsorb on their surface, guiding further cells behavior. Applying shorter time points in the MTT test (i.e., 1, 3 or 6 h) [74] could be an effective strategy to elucidate the initial effect of these nanoparticles in cell attachment. However, despite the initial levels of cell attachment, the main effect of nanoparticles on cells' viability is already observed at the first 24 h, with a decrease in an increase in cells' proliferation, but after 48 or 72 h, usually, a balance is acquired if the material is biocompatible. Therefore, we employed a 3-day MTT test as indicative of the materials' toxicity, although shorter or longer evaluation times would be more informative. In addition, further tests are needed to provide information on the mechanisms of cell damage or death and to explain the decreased biocompatibility of the nY-ZrO800 observed in this study. Despite the scientific knowledge related to cell death mechanisms, further work is needed to elucidate the toxicological behavior of the various nanomaterials and to clarify the particular factors that affect cell fate in their presence. Moreover, there is a need to evaluate if this biological behavior can affect cell viability when these nanoparticles are used as fillers in dental cement or adhesives. In this respect, in-depth analysis, as presented in the study of Pagano et al. [74], and the use of direct cytotoxicity tests on dental cement, adhesives or composites with nano zirconia nanoparticles fillers should be performed.

The antioxidant potential is an important characteristic of nanoparticles specifying their free oxygen radical scavenging activity and their ability to protect cells from oxidative damage. In the current study, all specimens showed a statistically significant reduction in ROS, indicating the free radical scavenging activity in 24 h, irrespectively of the NPs concentrations added. It seems that the tested nanofillers were effective in neutralizing oxidative stress by stabilizing a basal production of ROS. Recently, the pronounced scavenging activity of ZrO₂-CeO₂ nanoparticles attributed to their oxygen storage capacity was reported by Tsai et al. [75]. Another study found the enhanced antioxidant activity of Fe₃O₄ stabilized zirconia nanoparticles [76]. At the same time, several studies reported that non-stabilized ZrO₂ nanoparticles could generate ROS and damage the cellular components as well as the DNA [38,77]. Although a ROS scavenging mechanism due to the presence of oxygen vacancies in nanomaterials can contribute to those results [78], in the study by Alzahrani et al. [79], dose-dependent apoptosis and genotoxicity of YSZ nanoparticles in

human skin keratinocyte cells were correlated with an increase in reactive oxygen species production at concentrations higher compared with the present study (up to 60 µg/mL), suggesting that maybe other mechanisms control the overall ROS production and/or scavenging. Such diversity in results could probably be attributed to differences in applied protocols and cell lines, as well as the chemical reactivity of pure zirconia as compared to its yttria-stabilized form.

Many studies used pure zirconia nanoparticles to enhance the mechanical properties of dental restorative composites, to enhance the bond strength to dentin of dental cement and adhesive systems or to increase the radiopacity of dental adhesives (Table 4). A recent review outlined the beneficial role of the incorporation of nanocompounds in dental materials with regards to the promotion of their bond's stability [80].

Table 4. Studies involving zirconia nanoparticles in dental cement, composites and adhesives.

Authors	Zirconia Nanoparticles Type/Size (nm)	Amount of Filler (%) w.t.	Evaluated Property	Main Results
Dental Cements				
Gjorgievska et al. [81]	ZrO ₂ (80 nm) * Glass Ionomer Cement	2, 5, 10	-compressive strength element release profile	Increased compressive strength, no release of Al, Zr or Ti
Sajjad et al. [82]	ZrO ₂ (114 nm) * Glass Ionomer Cement	3, 5, 7, 9	-compressive strength -flexural strength -surface roughness	Increase in compressive and flexural strength
Alobiedy et al. [83]	ZrO ₂ (20 nm) * Glass Ionomer Cement	3, 5, 7	-compressive strength -micro-hardness -biaxial flexural strength wear rate loss	Favorable effect on biaxial flexural strength, micro-hardness, wear rate loss
Ab Rahman et al. [84]	ZrO ₂ (40 nm) * Glass Ionomer Cement	1, 3, 5, 7, 9, 15, 20	-hardness color	Increased hardness and aesthetics
Gjorgievska et al. [85]	ZrO ₂ (80 nm) * Glass Ionomer Cement	10	-compressive strength	Increased compressive strength
Li et al. [86]	ZrO ₂ (200 nm) * Tricalcium Cement	5, 10, 20, 30, 50	-mini-fracture toughness -bioactivity -cytotoxicity	Increase in biocompatibility
Rahimi et al. [87]	ZrO ₂ (<100 nm) * Portland cement	30	-viability of human dental pulp cells	Increased alkaline phosphatase activity in human dental pulp cells
Viapiana et al. [88]	ZrO ₂ (nanosize is not reported) * Portland cement	30	-Setting time -compressive strength -flow -film thickness -radiopacity -solubility -dimensional stability -formaldehyde release	Film thickness requires further reduction
Li et al. [89]	ZrO ₂ (50–75 nm) * Portland cement	20	-hydration chemistry	Biocompatibility not compromised. Accelerated hydration

Table 4. Cont.

Authors	Zirconia Nanoparticles Type/Size (nm)	Amount of Filler (%) w.t.	Evaluated Property	Main Results
Dental Composites				
Ilie et al. [90]	GO-ZrO ₂ HA-ZrO ₂ (10–40 nm)	0.3 GO-ZrO ₂ 15 HA-ZrO ₂	-light transmittance -flexural strength, modulus, Weibull parameters -plastic and elastic deformation parameters	-Improved mechanical properties -Optical properties require adjustments
Hesaraki et al. [91]	3-YSZ (≤100 nm)	5, 10	-flexural strength compressive strength	-Increase in mechanical strength
Wu et al. [92]	ZrO ₂ coated with Zr (OH) ₄ (50 nm)	10	-flexural strength -elastic modulus -Weibull analysis	-Improvement of mechanical properties
Dai et al. [30]	ZrO ₂ coated with Zr (OH) ₄ (50 nm)	2.5, 5, 7.5	-flexural strength -translucency	-5% wt presented the highest strength
Furman et al. [93]	Zirconium propoxide (<100 nm)	10, 20, 30	-flexural strength -fracture toughness	-Reduced flexural strength
Dental Adhesives				
Provenzi et al. [94]	ZrO ₂ (<25 nm)	0.5, 1, 4.8, 9.1	-degree of conversion -radiopacity -tensile bond strength softening in solvent	1 wt% led to a significantly higher degree of conversion
Martins et al. [95]	ZrO ₂ (20–30 nm)	15, 25, 30, 50	-micro-hardness radiopacity	Increased micro-hardness and radiopacity
Lohbauer et al. [32]	YSZ (20–50 nm)	5, 10, 15, 20	-micro-tensile -bond strength	Increasing concentration led to higher bond strength values

* = Type of cement in which the nanoparticles were incorporated.

Spherical YSZ nanoparticles of size ranging from 20 to 50 nm were previously produced by laser vaporization and incorporated in dental adhesives [32]. Zirconia nanoparticle incorporation into the primer or adhesive resin solution of a multi-purpose adhesive system increased the bond strength significantly to dentin, and even higher strength was achieved when increased amounts were incorporated into the primer. Martins et al. [95] incorporated pre-fabricated, commercially available ZrO₂ nanoparticles (20–30 nm) in dental adhesives and found increased radiopacity and micro-hardness.

It was also proposed that ZrO₂ nanoparticles can be incorporated in resin-based composite materials after appropriate silanization [96]. In the study by Kaizer et al. [96], the average particle size incorporated was 37.3 nm, and it increased to 81.2 nm following their silica coating. Nanohybrid resin composites with 40 nm zirconia nanoparticles presented improved and more stable physical properties compared with commercial dental composites or composites reinforced with nanosilica [97]. In a recent study, zirconia nanofillers were incorporated in bis-GMA composite resins [98] up to 5–20 wt%. SEM images indicated spherical particles with sizes ranging between 20 and 50 nm, and a significant increase in bending strength was recorded for the composites.

Experimentally reinforced glass ionomer cement has been described in the literature recently. Gjorgievska et al. [85] attempted the incorporation of ZrO₂ nanoparticles of

average size 80 nm in glass ionomer restorative cement and reported fewer air voids in all nanoparticle-containing cement, which resulted in fewer cracks within the matrix of the cement, increasing their strength. Laiteerapong et al. [99] manufactured restorative glass ionomer cement after incorporation of pre-fabricated zirconia nanoparticles of size under 100nm (ZrO_2) and investigated the genotoxicity of their eluates on human gingival fibroblasts. They used nano and micro-sized zirconia particles up to 10% *w/w* and concluded that zirconia modified GICs had no genotoxic effect on HGFs in vitro. Sajjad et al. [82] synthesized nano ZrO_2 - SiO_2 -HA, which was incorporated in Fuji IX GIC restorative material and detected particles comprising of spherical ZrO_2 and SiO_2 crystals and rod shape HA crystals.

Further studies showed that dental materials reinforced with ZrO_2 nanoparticles present cell proliferating and antimicrobial properties. Specifically, Silva et al. [100] used ZrO_2 nanoparticles to reinforce a calcium silicate-based cement and observed an increase in fibroblast proliferation and reduced duration of the inflammatory response by rat fibroblasts. In the study by Bosso-Martelo et al. [101], 74 nm-sized ZrO_2 were incorporated into calcium silicate-based cement, resulting in bioactive materials, as evidenced by the hydroxyapatite precipitates on the surface of the specimens. In restorative glass ionomer cement, relative biocompatibility to human gingival fibroblasts was reported by Laiteerapong et al. [99]. Antimicrobial effects against microorganisms found in the oral cavity, particularly against Gram-negative bacteria, were reported by Fathima et al. [12]. In their study, particles synthesized by a method involving precipitation presented irregular spherical or spherical shapes, and their size ranged between 15 and 21 nm. The findings above indicate that the applied synthesis method in the present study led to smaller YSZ particle sizes (10–15 nm and 30–50 nm, respectively, for sintering temperatures of 800 °C and 1000 °C) when comparing them to the ZrO_2 nanoparticles used in most studies.

It can be assumed that the favorable biological properties and crystallographic characteristics observed in the present study could allow applications of these nanoparticles in dental materials that require strict working times, viscosity and film thickness, such as luting cement. Other applications could include restorative materials as well as dental adhesives and root-end filling materials. The existing evidence on their biological and mechanical properties is promising with regards to their use as optimized fillers. However, this study has some limitations. A more detailed analysis should be performed in terms of explaining the underlying mechanisms of cells response and the differences depending on the sintering temperature. A more detailed TEM analysis on the nY-ZrO800 and nY-ZrO1200 should provide clarifying information on the role of any particular structural and morphological characteristics of nanoparticles on their biological response and ROS production to allow optimization of their production. Their biocompatibility should also be evaluated in comparison with pure ZrO_2 nanoparticles to elucidate any potential effect of yttrium in their composition. Future studies in light of the above and the use of other cell lines such as dental pulp stem cells should be considered for conclusive results.

In the present study, yttrium stabilized zirconia nanoparticles were synthesized through a sol-gel-based method, and their biocompatibility were evaluated after sintering at various temperatures. As a different biological behavior was observed depending on sintering temperature, the null hypothesis was rejected.

5. Conclusions

Pure tetragonal YSZ nanopowders with low agglomeration were successfully synthesized by the sol-gel method at different temperatures. The size and crystallographic characteristics of the synthesized nanoparticles suggest the heat treatment at temperatures ≤ 1000 °C can lead to optimum properties, making YSZ nanoparticles potentially suitable as nanofillers for resin luting cement in dentistry. The results of the present study suggest that the sol-gel method is an effective alternative to traditional high-temperature synthesis techniques for the stabilization of the tetragonal zirconia at room temperature and the elimination of any monoclinic traces.

Author Contributions: Conceptualization, A.E.R. and E.K.; methodology, A.B., A.T. and I.T.; validation, E.-G.C.T.; formal analysis, G.K.P., L.L., D.K., M.A.O., A.A. and I.T.; investigation, A.B., G.K.P., E.-G.C.T., A.A. and I.T.; data curation, E.K.; writing—original draft preparation, A.B., A.E.R. and I.T.; writing—review and editing, E.K.; visualization, G.K.P., L.L. and D.K.; supervision, E.K. and I.G.T.; project administration, E.K. and I.G.T.; funding acquisition, E.K. All authors have read and agreed to the published version of the manuscript.

Funding: This research was co-financed by Greece and European Union (EUROPEAN SOCIAL FUND-ESF), through the Operational Program “Human Resources Development, Education, and Lifelong Learning 2014–2020” in the context of the project “Development of zirconia adhesion cements with stabilized zirconia nanoparticles: physicochemical properties and bond strength under aging conditions” grant number MIS5047876.



Operational Programme
Human Resources Development,
Education and Lifelong Learning
Co-financed by Greece and the European Union



Institutional Review Board Statement: The study was conducted according to the guidelines of the Declaration of Helsinki and approved by the Ethics Committee of the School of Dentistry, Aristotle University of Thessaloniki, Greece (#35/07-05-2018).

Informed Consent Statement: Informed consent was obtained from all subjects involved in the study.

Data Availability Statement: Data is contained within the article.

Acknowledgments: The authors would like to acknowledge Konstantinos Simeonidis for XRD analysis and Triantafyllia Zorba for assistance in FTIR analysis. The authors want to thank Konstantinos Chrysafis for providing the facilities of the Laboratory of Advanced Materials and Devices at Aristotle University of Thessaloniki (<http://amdelab.physics.auth.gr/members-en.htm>, 27 October 2021). The authors thank Aldo R. Boccaccini for granting access to the facilities (SEM-EDX and DLS analyses) at the Institute of Biomaterials, Department of Materials Science and Engineering, University of Erlangen-Nuremberg.

Conflicts of Interest: The authors declare no conflict of interest.

References

- Gautam, C.; Joyner, J.; Gautam, A.; Rao, J.; Vajtai, R. Zirconia based dental ceramics: Structure, mechanical properties, biocompatibility and applications. *Dalt. Trans.* **2016**, *45*, 19194–19215. [CrossRef] [PubMed]
- Vagkopoulou, T.; Koutayas, S.O.; Koidis, P.; Strub, J.R. Zirconia in dentistry: Part 1. Discovering the nature of an upcoming bioceramic. *Eur. J. Esthet. Dent.* **2009**, *4*, 130–151. [PubMed]
- Koutayas, S.O.; Vagkopoulou, T.; Pelekanos, S.; Koidis, P.; Strub, J.R. Zirconia in dentistry: Part 2. Evidence-based clinical breakthrough. *Eur. J. Esthet. Dent.* **2009**, *4*, 348–380. [PubMed]
- Habib, E.; Wang, R.; Wang, Y.; Zhu, M.; Zhu, X.X. Inorganic Fillers for Dental Resin Composites: Present and Future. *ACS Biomater. Sci. Eng.* **2016**, *2*, 1–11. [CrossRef]
- Wang, T.; Tsoi, J.K.H.; Matinlinna, J.P. A novel zirconia fibre-reinforced resin composite for dental use. *J. Mech. Behav. Biomed. Mater.* **2016**, *53*, 151–160. [CrossRef]
- Das, I.; Chattopadhyay, S.; Mahato, A.; Kundu, B.; De, G. Fabrication of a cubic zirconia nanocoating on a titanium dental implant with excellent adhesion, hardness and biocompatibility. *RSC Adv.* **2016**, *6*, 59030–59038. [CrossRef]
- Hu, C.; Sun, J.; Long, C.; Wu, L.; Zhou, C.; Zhang, X. Synthesis of nano zirconium oxide and its application in dentistry. *Nanotechnol. Rev.* **2019**, *8*, 396–404. [CrossRef]
- Guerreiro Tanomaru, J.M.; Storto, I.; da Silva, G.F.; Bosso, R.; Costa, B.C.; Bernardi, M.I.B.; Tanomaru-Filho, M. Radiopacity, pH and antimicrobial activity of Portland cement associated with micro- and nanoparticles of zirconium oxide and niobium oxide. *Dent. Mater. J.* **2014**, *33*, 466–470. [CrossRef]
- Bortoluzzi, E.A.; Guerreiro-Tanomaru, J.M.; Tanomaru-Filho, M.; Duarte, M.A.H. Radiographic effect of different radiopacifiers on a potential retrograde filling material. *Oral Surg. Oral Med. Oral Pathol. Oral Radiol. Endodontology* **2009**, *108*, 628–632. [CrossRef]
- Gad, M.M.; Rahoma, A.; Al-Thobity, A.M.; ArRejaie, A.S. Influence of incorporation of ZrO₂ nanoparticles on the repair strength of polymethyl methacrylate denture bases. *Int. J. Nanomed.* **2016**, *11*, 5633–5643. [CrossRef]
- Yang, J.; Shen, J.; Wu, X.; He, F.; Xie, H.; Chen, C. Effects of nano-zirconia fillers conditioned with phosphate ester monomers on the conversion and mechanical properties of Bis-GMA- and UDMA-based resin composites. *J. Dent.* **2020**, *94*, 103306. [CrossRef]

12. Fathima, J.B.; Pugazhendhi, A.; Venis, R. Synthesis and characterization of ZrO₂ nanoparticles-antimicrobial activity and their prospective role in dental care. *Microb. Pathog.* **2017**, *110*, 245–251. [[CrossRef](#)]
13. Souza, J.C.M.; Silva, J.B.; Aladim, A.; Carvalho, O.; Nascimento, R.M.; Silva, F.S.; Martinelli, A.E.; Henriques, B. Effect of Zirconia and Alumina Fillers on the Microstructure and Mechanical Strength of Dental Glass Ionomer Cements. *Open Dent. J.* **2016**, *10*, 58–68. [[CrossRef](#)]
14. Lyon, D.; Chevalier, J.; Gremillard, L.; Cam, C.a.D. Zirconia as a Biomaterial. *Compr. Biomater.* **2011**, *20*, 95–108. [[CrossRef](#)]
15. Chevalier, J. What future for zirconia as a biomaterial? *Biomaterials* **2006**, *27*, 535–543. [[CrossRef](#)]
16. Chevalier, J.J.; Gremillard, L.; Virkar, A.V.; Clarke, D.R. The tetragonal-monoclinic transformation in zirconia: Lessons learned and future trends. *J. Am. Ceram. Soc.* **2009**, *92*, 1901–1920. [[CrossRef](#)]
17. Piconi, C.; Maccauro, G. Zirconia as a ceramic biomaterial. *Biomaterials* **1999**, *20*, 1–25. [[CrossRef](#)]
18. Chevalier, J.; Gremillard, L.; Deville, S. Low-Temperature Degradation of Zirconia and Implications for Biomedical Implants. *Annu. Rev. Mater. Res.* **2007**, *37*, 1–32. [[CrossRef](#)]
19. Sheu, T.-S.; Tien, T.-Y.; Chen, I.-W. Cubic-to-Tetragonal (t') Transformation in Zirconia-Containing Systems. *J. Am. Ceram. Soc.* **1992**, *75*, 1108–1116. [[CrossRef](#)]
20. Bona, A.D.; Pecho, O.E.; Alessandretti, R. Zirconia as a Dental Biomaterial. *Materials* **2015**, *8*, 4978–4991. [[CrossRef](#)]
21. Kontonasaki, E.; Giasimakopoulos, P.; Rigos, A.E. Strength and aging resistance of monolithic zirconia: An update to current knowledge. *Jpn. Dent. Sci. Rev.* **2020**, *56*, 1–23. [[CrossRef](#)]
22. Vasylyk, O.; Sakka, Y. Synthesis and colloidal processing of zirconia nanopowder. *J. Am. Ceram. Soc.* **2001**, *84*, 2489–2494. [[CrossRef](#)]
23. Tok, A.I.Y.; Boey, F.Y.C.; Du, S.W.; Wong, B.K. Flame spray synthesis of ZrO₂ nano-particles using liquid precursors. *Mater. Sci. Eng. B Solid-State Mater. Adv. Technol.* **2006**, *130*, 114–119. [[CrossRef](#)]
24. Hajizadeh-Oghaz, M.; Razavi, R.S.; Estarki, M.L. Large-scale synthesis of YSZ nanopowder by Pechini method. *Bull. Mater. Sci.* **2014**, *37*, 969–973. [[CrossRef](#)]
25. Sagadevan, S.; Podder, J.; Das, I. Hydrothermal synthesis of zirconium oxide nanoparticles and its characterization. *J. Mater. Sci. Mater. Electron.* **2016**, *27*, 5622–5627. [[CrossRef](#)]
26. Heshmatpour, F.; Khodaiy, Z.; Aghakhanpour, R.B. Synthesis and characterization of pure tetragonal nanocrystalline sulfated 8YSZ powder by sol-gel route. *Powder Technol.* **2012**, *224*, 12–18. [[CrossRef](#)]
27. Hsu, Y.W.; Yang, K.H.; Chang, K.M.; Yeh, S.W.; Wang, M.C. Synthesis and crystallization behavior of 3 mol% yttria stabilized tetragonal zirconia polycrystals (3Y-TZP) nanosized powders prepared using a simple co-precipitation process. *J. Alloys Compd.* **2011**, *509*, 6864–6870. [[CrossRef](#)]
28. Sato, K.; Horiguchi, K.; Nishikawa, T.; Yagishita, S.; Kuruma, K.; Murakami, T.; Abe, H. Hydrothermal Synthesis of Yttria-Stabilized Zirconia Nanocrystals with Controlled Yttria Content. *Inorg. Chem.* **2015**, *54*, 7976–7984. [[CrossRef](#)]
29. Gonzalo-Juan, I.; Ferrari, B.; Colomer, M.T. Influence of the urea content on the YSZ hydrothermal synthesis under dilute conditions and its role as dispersant agent in the post-reaction medium. *J. Eur. Ceram. Soc.* **2009**, *29*, 3185–3195. [[CrossRef](#)]
30. Dai, S.; Chen, Y.; Yang, J.; He, F.; Chen, C.; Xie, H. Surface treatment of nanozirconia fillers to strengthen dental bisphenol a-glycidyl methacrylate-based resin composites. *Int. J. Nanomed.* **2019**, *14*, 9185–9197. [[CrossRef](#)]
31. Alhaleb, A.O.; Akil, H.M.; Ahmad, Z.A. Impact strength, fracture toughness and hardness improvement of PMMA denture base through addition of nitrile rubber/ceramic fillers. *Saudi. J. Dent. Res.* **2017**, *8*, 26–34. [[CrossRef](#)]
32. Lohbauer, U.; Wagner, A.; Belli, R.; Stoetzel, C.; Hilpert, A.; Kurland, H.D.; Grabow, J.; Müller, F.A. Zirconia nanoparticles prepared by laser vaporization as fillers for dental adhesives. *Acta Biomater.* **2010**, *6*, 4539–4546. [[CrossRef](#)] [[PubMed](#)]
33. Hajizadeh-Oghaz, M.; Shoja Razavi, R.; Loghman-Estarki, M.R. Synthesis and characterization of non-transformable tetragonal YSZ nanopowder by means of Pechini method for thermal barrier coatings (TBCs) applications. *J. Sol.-Gel Sci. Technol.* **2014**, *70*, 6–13. [[CrossRef](#)]
34. Tailor, S.; Singh, M.; Doub, A.V. Synthesis and Characterization of Yttria-Stabilized Zirconia (YSZ) Nano-Clusters for Thermal Barrier Coatings (TBCs) Applications. *J. Clust. Sci.* **2016**, *27*, 1097–1107. [[CrossRef](#)]
35. Aly, K.A.; Khalil, N.M.; Algarni, Y.; Saleem, Q.M.A. Estimation of lattice strain for zirconia nano-particles based on Williamson-Hall analysis. *Mater. Chem. Phys.* **2017**, *193*, 182–188. [[CrossRef](#)]
36. Wu, X.; Landheer, D.; Graham, M.J.; Chen, H.W.; Huang, T.Y.; Chao, T.S. Structure and thermal stability of MOCVD ZrO₂ films on Si (1 0 0). *J. Cryst. Growth* **2003**, *250*, 479–485. [[CrossRef](#)]
37. Karunakaran, G.; Suriyaprabha, R.; Manivasakan, P.; Yuvakkumar, R.; Rajendran, V.; Kannan, N. Screening of in vitro cytotoxicity, antioxidant potential and bioactivity of nano- and micro-ZrO₂ and -TiO₂ particles. *Ecotoxicol. Environ. Saf.* **2013**, *93*, 191–197. [[CrossRef](#)]
38. Asadpour, E.; Sadeghnia, H.R.; Ghorbani, A.; Sedaghat, M.; Boroushaki, M.T. Oxidative stress-mediated cytotoxicity of zirconia nanoparticles on PC12 and N2a cells. *J. Nanoparticle Res.* **2016**, *18*, 1–13. [[CrossRef](#)]
39. Avalos, A.; Haza, A.I.; Mateo, D.; Morales, P. Interactions of manufactured silver nanoparticles of different sizes with normal human dermal fibroblasts. *Int. Wound J.* **2016**, *13*, 101–109. [[CrossRef](#)]
40. Tsamesidis, I.; Reybier, K.; Marchetti, G.; Pau, M.C.; Viridis, P.; Fozza, C.; Nepveu, F.; Low, P.S.; Turrini, F.M.; Pantaleo, A. Syk kinase inhibitors synergize with artemisinin by enhancing oxidative stress in plasmodium falciparum-parasitized erythrocytes. *Antioxidants* **2020**, *9*, 753. [[CrossRef](#)]

41. Halmenschlager, C.M.; Vieira, R.; Falcade, T. Characterization of Cubic Yttria-Stabilized. In Proceedings of the International Latin-American Conference on Powder Technology, Atibaia, Brazil, 8–10 November 2009; pp. 890–895.
42. Courtin, E.; Boy, P.; Rouhet, C.; Bianchi, L.; Bruneton, E.; Poirot, N.; Laberty-Robert, C.; Sanchez, C. Optimized Sol-Gel Routes to Synthesize Yttria-Stabilized Zirconia Thin Films as Solid Electrolytes for Solid Oxide Fuel Cells. *Chem. Mater.* **2012**, *24*, 4540–4548. [[CrossRef](#)]
43. Judes, J.; Kamaraj, V. Preparation and characterization of yttria stabilized zirconia minispheres by the sol-gel drop generation method. *Mater. Sci. Pol.* **2009**, *27*, 407–415.
44. Zarkov, A.; Stanulis, A.; Sakaliuniene, J.; Butkute, S.; Abakeviciene, B.; Salkus, T.; Tautkus, S.; Orliukas, A.F.; Tamulevicius, S.; Kareiva, A. On the synthesis of yttria-stabilized zirconia: A comparative study. *J. Sol.-Gel Sci. Technol.* **2015**, *76*, 309–319. [[CrossRef](#)]
45. Huang, Z.; Han, W.; Feng, Z.; Qi, J.; Wu, D.; Wei, N.; Tang, Z.; Zhang, Y.; Duan, J.; Lu, T. The effects of precipitants on co-precipitation synthesis of yttria-stabilized zirconia nanocrystalline powders. *J. Sol-Gel Sci. Technol.* **2019**, *90*, 359–368. [[CrossRef](#)]
46. Fernandez Lopez, E.; Sanchez Escribano, V.; Panizza, M.; Carnasciali, M.M.; Busca, G. Vibrational and electronic spectroscopic properties of zirconia powders. *J. Mater. Chem.* **2001**, *11*, 1891–1897. [[CrossRef](#)]
47. Niu, X.; Xie, M.; Zhou, F.; Mu, R.; Song, X.; An, S. Substituent influence of yttria by gadolinia on the tetragonal phase stability for Y_2O_3 - Ta_2O_5 - ZrO_2 ceramics at 1300 °C. *J. Mater. Sci. Technol.* **2014**, *30*, 381–386. [[CrossRef](#)]
48. Srinivasan, R.; De Angelis, R.J.; Ice, G.; Davis, B.H. Identification of tetragonal and cubic structures of zirconia using synchrotron x-radiation source. *J. Mater. Res.* **1991**, *6*, 1287–1292. [[CrossRef](#)]
49. Zhang, F.; Reveron, H.; Spies, B.C.; Van Meerbeek, B.; Chevalier, J. Trade-off between fracture resistance and translucency of zirconia and lithium-disilicate glass ceramics for monolithic restorations. *Acta Biomater.* **2019**, *91*, 24–34. [[CrossRef](#)]
50. Kumari, L.; Li, W.Z.; Xu, J.M.; Leblanc, R.M.; Wang, D.Z.; Li, Y.; Guo, H.; Zhang, J. Controlled hydrothermal synthesis of zirconium oxide nanostructures and their optical properties. *Cryst. Growth Des.* **2009**, *9*, 3874–3880. [[CrossRef](#)]
51. Zong, S.; Cao, Y.; Zhou, Y.; Ju, H. Zirconia nanoparticles enhanced grafted collagen tri-helix scaffold for unmediated biosensing of hydrogen peroxide. *Langmuir* **2006**, *22*, 8915–8919. [[CrossRef](#)]
52. Pérez-Tanoira, R.; Horwat, D.; Kinnari, T.J.; Pérez-Jorge, C.; Gómez-Barrena, E.; Migot, S.; Esteban, J. Bacterial adhesion on biomedical surfaces covered by yttria stabilized zirconia. *J. Mater. Sci. Mater. Med.* **2016**, *27*, 1–9. [[CrossRef](#)] [[PubMed](#)]
53. Lahwal, A.; Bhattacharya, S.; He, J.; Wu, D.; Peterson, A.; Poon, S.J.; Williams, L.; Dehkordi, A.M.; Tritt, T.M. Impact of yttria stabilized zirconia nano-inclusions on the thermal conductivity of n-type Si80 Ge20 alloys prepared by spark plasma sintering. *J. Appl. Phys.* **2015**, *117*, 145101. [[CrossRef](#)]
54. Maridurai, T.; Balaji, D.; Sagadevan, S. Synthesis and Characterization of Yttrium Stabilized Zirconia Nanoparticles. *Mater. Res.* **2016**, *19*, 812–816. [[CrossRef](#)]
55. Bahamirian, M.; Hadavi, S.M.M.; Rahimipour, M.R.; Farvizi, M.; Keyvani, A. Synthesis and Characterization of Yttria-Stabilized Zirconia Nanoparticles Doped with Ytterbium and Gadolinium: $ZrO_{2.9.5}Y_{2.0.3}Yb_{2.0.3}5.2Gd_{2.0.3}$. *Metall. Mater. Trans. A Phys. Metall. Mater. Sci.* **2018**, *49*, 2523–2532. [[CrossRef](#)]
56. Khajavi, P.; Xu, Y.; Frandsen, H.L.; Chevalier, J.; Gremillard, L.; Kiebach, R.; Hendriksen, P.V. Tetragonal phase stability maps of ceria-yttria co-doped zirconia: From powders to sintered ceramics. *Ceram. Int.* **2020**, *46*, 9396–9405. [[CrossRef](#)]
57. Garvie, R.C. The occurrence of metastable tetragonal zirconia as a crystallite size effect. *J. Phys. Chem.* **1965**, *69*, 1238–1243. [[CrossRef](#)]
58. Chraska, T.; King, A.H.; Berndt, C.C. On the size-dependent phase transformation in nanoparticulate zirconia. *Mater. Sci. Eng. A* **2000**, *286*, 169–178. [[CrossRef](#)]
59. Nitsche, R.; Winterer, M.; Hahn, H. Structure of nanocrystalline zirconia and yttria. *Nanostructured Mater.* **1995**, *6*, 679–682. [[CrossRef](#)]
60. Shukla, S.; Seal, S. Mechanisms of room temperature metastable tetragonal phase stabilisation in zirconia. *Int. Mater. Rev.* **2005**, *50*, 45–64. [[CrossRef](#)]
61. Tsunekawa, S.; Ito, S.; Kawazoe, Y.; Wang, J.T. Critical size of the phase transition from cubic to tetragonal in pure zirconia nanoparticles. *Nano Lett.* **2003**, *3*, 871–875. [[CrossRef](#)]
62. Chatterjee, A.; Pradhan, S.K.; Datta, A.; De, M.; Chakravorty, D. Stability of Cubic Phase in Nanocrystalline ZrO_2 . *J. Mater. Res.* **1994**, *9*, 263–265. [[CrossRef](#)]
63. Lu, K. Sintering of nanoceramics. *Int. Mater. Rev.* **2008**, *53*, 21–38. [[CrossRef](#)]
64. Maca, K.; Trunec, M.; Dobsak, P. Bulk zirconia nanoceramics prepared by cold isostatic pressing and pressureless sintering. *Rev. Adv. Mater. Sci.* **2005**, *10*, 84–88.
65. Stolzenburg, P.; Hämisch, B.; Richter, S.; Huber, K.; Garnweitner, G. Secondary Particle Formation during the Nonaqueous Synthesis of Metal Oxide Nanocrystals. *Langmuir* **2018**, *34*, 12834–12844. [[CrossRef](#)]
66. Tobler, D.J.; Shaw, S.; Benning, L.G. Quantification of initial steps of nucleation and growth of silica nanoparticles: An in-situ SAXS and DLS study. *Geochim. Cosmochim. Acta* **2009**, *73*, 5377–5393. [[CrossRef](#)]
67. Tomaszewska, E.; Soliwoda, K.; Kadziola, K.; Tkacz-Szczesna, B.; Celichowski, G.; Cichomski, M.; Szmaja, W.; Grobelny, J. Detection limits of DLS and UV-Vis spectroscopy in characterization of polydisperse nanoparticles colloids. *J. Nanomater.* **2013**, *2013*, 60. [[CrossRef](#)]

68. Pabisch, S.; Feichtenschlager, B.; Kickelbick, G.; Peterlik, H. Effect of interparticle interactions on size determination of zirconia and silica based systems—A comparison of SAXS, DLS, BET, XRD and TEM. *Chem. Phys. Lett.* **2012**, *521*, 91–97. [[CrossRef](#)]
69. Sukhanova, A.; Bozrova, S.; Sokolov, P.; Berestovoy, M.; Karaulov, A.; Nabiev, I. Dependence of Nanoparticle Toxicity on Their Physical and Chemical Properties. *Nanoscale Res. Lett.* **2018**, *13*, 44. [[CrossRef](#)]
70. Pan, Y.; Neuss, S.; Leifert, A.; Fischler, M.; Wen, F.; Simon, U.; Schmid, G.; Brandau, W.; Jahnen-Dechent, W. Size-dependent cytotoxicity of gold nanoparticles. *Small* **2007**, *3*, 1941–1949. [[CrossRef](#)]
71. Zhang, Y.F.; Zheng, Y.F.; Qin, L. A comprehensive biological evaluation of ceramic nanoparticles as wear debris. *Nanomed. Nanotechnol. Biol. Med.* **2011**, *7*, 975–982. [[CrossRef](#)]
72. Wang, J.; Yin, W.; He, X.; Wang, Q.; Guo, M.; Chen, S. Good Biocompatibility and Sintering Properties of Zirconia Nanoparticles Synthesized via Vapor-phase Hydrolysis. *Sci. Rep.* **2016**, *6*, 35020. [[CrossRef](#)] [[PubMed](#)]
73. Rutherford, D.; Exarhos, S.; Xu, C.; Niacaris, M.; Mariano, C.; Dayap, B.; Mangolini, L.; Liu, H. Synthesis, characterization, and cytocompatibility of yttria stabilized zirconia nanopowders for creating a window to the brain. *J. Biomed. Mater. Res. Part. B Appl. Biomater.* **2020**, *108*, 925–938. [[CrossRef](#)] [[PubMed](#)]
74. Pagano, S.; Lombardo, G.; Costanzi, E.; Balloni, S.; Bruscoli, S.; Flamini, S.; Coniglio, M.; Valenti, C.; Cianetti, S.; Marinucci, L. Morpho-functional effects of different universal dental adhesives on human gingival fibroblasts: An in vitro study. *Odontology* **2021**, *109*, 524–539. [[CrossRef](#)] [[PubMed](#)]
75. Tsai, Y.Y.; Oca-Cossio, J.; Lin, S.M.; Woan, K.; Yu, P.C.; Sigmund, W. Reactive oxygen species scavenging properties of ZrO₂-CeO₂ solid solution nanoparticles. *Nanomedicine* **2008**, *3*, 637–645. [[CrossRef](#)]
76. Imran, M.; Riaz, S.; Shah, S.M.H.; Batool, T.; Khan, H.N.; Sabri, A.N.; Naseem, S. In-vitro hemolytic activity and free radical scavenging by sol-gel synthesized Fe₃O₄ stabilized ZrO₂ nanoparticles. *Arab. J. Chem.* **2020**, *13*, 7598–7608. [[CrossRef](#)]
77. Atalay, H.; Çelik, A.; Ayaz, F. Investigation of genotoxic and apoptotic effects of zirconium oxide nanoparticles (20 nm) on L929 mouse fibroblast cell line. *Chem. Biol. Interact.* **2018**, *296*, 98–104. [[CrossRef](#)]
78. Gunawan, C.; Lord, M.S.; Lovell, E.; Wong, R.J.; Jung, M.S.; Oscar, D.; Mann, R.; Amal, R. Oxygen-Vacancy Engineering of Cerium-Oxide Nanoparticles for Antioxidant Activity. *ACS Omega* **2019**, *4*, 9473–9479. [[CrossRef](#)]
79. Alzahrani, F.M.; Katubi, K.M.S.; Ali, D.; Alarifi, S. Apoptotic and DNA-damaging effects of yttrium-stabilized zirconia nanoparticles on human skin epithelial cells. *Int. J. Nanomed.* **2019**, *14*, 7003–7016. [[CrossRef](#)]
80. Münchow, E.A.; Bottino, M.C. Recent Advances in Adhesive Bonding: The Role of Biomolecules, Nanocompounds, and Bonding Strategies in Enhancing Resin Bonding to Dental Substrates. *Curr. Oral Heal. Rep.* **2017**, *4*, 215–227. [[CrossRef](#)]
81. Gjorgievska, E.; Nicholson, J.W.; Gabrić, D.; Guclu, Z.A.; Miletić, I.; Coleman, N.J. Assessment of the impact of the addition of nanoparticles on the properties of glass-ionomer cements. *Materials* **2020**, *13*, 276. [[CrossRef](#)]
82. Sajjad, A.; Bakar, W.Z.W.; Mohamad, D.; Kannan, T.P. Characterization and enhancement of physico-mechanical properties of glass ionomer cement by incorporating a novel nano zirconia silica hydroxyapatite composite synthesized via sol-gel. *AIMS Mater. Sci.* **2019**, *6*, 730–747. [[CrossRef](#)]
83. Alobiedy, A.N.; Alhille, A.H.; Al-Hamaoy, A.R. Mechanical Properties Enhancement of Conventional Glass Ionomer Cement by Adding Zirconium Oxide Micro and Nanoparticles. *J. Eng.* **2019**, *25*, 72–81. [[CrossRef](#)]
84. Rahman, I.A.; Ghazali, N.A.M.; Bakar, W.Z.W.; Masudi, S.M. Modification of glass ionomer cement by incorporating nanozirconia-hydroxyapatite-silica nano-powder composite by the one-pot technique for hardness and aesthetics improvement. *Ceram. Int.* **2017**, *43*, 13247–13253. [[CrossRef](#)]
85. Gjorgievska, E.; Van Tendeloo, G.; Nicholson, J.W.; Coleman, N.J.; Slipper, I.J.; Booth, S. The Incorporation of Nanoparticles into Conventional Glass-Ionomer Dental Restorative Cements. *Microsc. Microanal.* **2015**, *21*, 392–406. [[CrossRef](#)]
86. Li, X.; Yoshihara, K.; De Munck, J.; Cokic, S.; Pongprueksa, P.; Putzeys, E.; Pedano, M.; Chen, Z.; Van Landuyt, K.; Van Meerbeek, B. Modified tricalcium silicate cement formulations with added zirconium oxide. *Clin. Oral Investig.* **2017**, *21*, 895–905. [[CrossRef](#)]
87. Rahimi, S.; Salarinasab, S.; Ghasemi, N.; Rahbarghazi, R.; Shahi, S.; Salem Milani, A.; Divband, B.; Davoudi, P. In vitro induction of odontogenic activity of human dental pulp stem cells by white Portland cement enriched with zirconium oxide and zinc oxide components. *J. Dent. Res. Dent. Clin. Dent. Prospect.* **2019**, *13*, 3–10. [[CrossRef](#)]
88. Viapiana, R.; Flumignan, D.L.; Guerreiro-Tanomaru, J.M.; Camilleri, J.; Tanomaru-Filho, M. Physicochemical and mechanical properties of zirconium oxide and niobium oxide modified Portland cement-based experimental endodontic sealers. *Int. Endod. J.* **2014**, *47*, 437–448. [[CrossRef](#)]
89. Li, Q.; Deacon, A.D.; Coleman, N.J. The impact of zirconium oxide nanoparticles on the hydration chemistry and biocompatibility of white Portland cement. *Dent. Mater. J.* **2013**, *32*, 808–815. [[CrossRef](#)]
90. Ilie, N.; Sarosi, C.; Rosu, M.C.; Moldovan, M. Synthesis and characterization of graphene oxide-zirconia (GO-ZrO₂) and hydroxyapatite-zirconia (HA-ZrO₂) nano-fillers for resin-based composites for load-bearing applications. *J. Dent.* **2021**, *105*, 103557. [[CrossRef](#)]
91. Hesarakhi, S.; Karimi, M.; Nezafati, N. The synergistic effects of SrF₂ nanoparticles, YSZ nanoparticles, and poly-ε-L-lysine on physicochemical, ion release, and antibacterial-cellular behavior of the flowable dental composites. *Mater. Sci. Eng. C* **2020**, *109*, 110592. [[CrossRef](#)]
92. Wu, X.; Dai, S.; Chen, Y.; He, F.; Xie, H.; Chen, C. Reinforcement of dental resin composite via zirconium hydroxide coating and phosphate ester monomer conditioning of nano-zirconia fillers. *J. Mech. Behav. Biomed. Mater.* **2019**, *94*, 32–41. [[CrossRef](#)]

93. Furman, B.; Ralph Rawls, H.; Wellinghoff, S.; Dixon, H.; Lankford, J.; Nicoletta, D. Metal-oxide nanoparticles for the reinforcement of dental restorative resins. *Crit. Rev. Biomed. Eng.* **2000**, *28*, 439–443. [[CrossRef](#)]
94. Provenzi, C.; Collares, F.M.; Cuppini, M.; Samuel, S.M.W.; Alves, A.K.; Bergmann, C.P.; Leitune, V.C.B. Effect of nanostructured zirconium dioxide incorporation in an experimental adhesive resin. *Clin. Oral Investig.* **2018**, *22*, 2209–2218. [[CrossRef](#)]
95. Martins, G.C.; Meier, M.M.; Loguercio, A.D.; Cecchin, F.; Gomes, O.M.M.; Reis, A. Effects of zirconia nanoparticles addition to experimental adhesives on radiopacity and microhardness. *Braz. J. Oral Sci.* **2013**, *12*, 319–322. [[CrossRef](#)]
96. Kaizer, M.R.; Almeida, J.R.; Gonçalves, A.P.R.; Zhang, Y.; Cava, S.S.; Moraes, R.R. Silica coating of nonsilicate nanoparticles for resin-based composite materials. *J. Dent. Res.* **2016**, *95*, 1394–1400. [[CrossRef](#)]
97. Nakanishi, L.; Kaizer, M.R.; Brandeburski, S.; Cava, S.S.; Della Bona, A.; Zhang, Y.; Moraes, R.R. Non-silicate nanoparticles for improved nanohybrid resin composites. *Dent. Mater.* **2020**, *36*, 1314–1321. [[CrossRef](#)]
98. Hong, G.; Yang, J.; Jin, X.; Wu, T.; Dai, S.; Xie, H.; Chen, C. Mechanical Properties of Nanohybrid Resin Composites Containing Various Mass Fractions of Modified Zirconia Particles. *Int. J. Nanomed.* **2020**, *15*, 9891. [[CrossRef](#)]
99. Laiteerapong, A.; Reichl, F.X.; Hickel, R.; Högg, C. Effect of eluates from zirconia-modified glass ionomer cements on DNA double-stranded breaks in human gingival fibroblast cells. *Dent. Mater.* **2019**, *35*, 444–449. [[CrossRef](#)]
100. Silva, G.F.; Guerreiro-Tanomaru, J.M.; da Fonseca, T.S.; Bernardi, M.I.B.; Sasso-Cerri, E.; Tanomaru-Filho, M.; Cerri, P.S. Zirconium oxide and niobium oxide used as radiopacifiers in a calcium silicate-based material stimulate fibroblast proliferation and collagen formation. *Int. Endod. J.* **2017**, *50*, e95–e108. [[CrossRef](#)]
101. Bosso-Martelo, R.; Guerreiro-Tanomaru, J.M.; Viapiana, R.; Berbert, F.L.C.V.; Basso Bernardi, M.I.; Tanomaru-Filho, M. Calcium Silicate-Based Cements Associated with Micro- and Nanoparticle Radiopacifiers: Physicochemical Properties and Bioactivity. *Int. Sch. Res. Not.* **2015**, *2015*, 1–7. [[CrossRef](#)]